

Cite this: *Catal. Sci. Technol.*, 2021,
11, 7751

Exploration of highly electron-rich manganese complexes in enantioselective oxidation catalysis; a focus on enantioselective benzylic oxidation†

Eduard Masferrer-Rius,^a Fanshi Li,^a
Martin Lutz^b and Robertus J. M. Klein Gebbink^b*^a

The direct enantioselective hydroxylation of benzylic C–H bonds to form chiral benzylic alcohols represents a challenging transformation. Herein, we report on the exploration of new biologically inspired manganese and iron complexes bearing highly electron-rich aminopyridine ligands containing 4-pyrrolidinopyridine moieties ((*S,S*)-**1**, (*R,R*)-**1**, **2** and **5**) in combination with chiral bis-pyrrolidine and *N,N*-cyclohexanediamine backbones in enantioselective oxidation catalysis with aqueous H₂O₂. The current manganese complexes outperform the analogous manganese complexes containing 4-dimethylaminopyridine moieties (**3** and **4**) in benzylic oxidation reactions in terms of alcohol yield while keeping similar ee values (~60% ee), which is attributed to the higher basicity of the 4-pyrrolidinopyridine group. A detailed investigation of different carboxylic acid additives in enantioselective benzylic oxidation provides new insights into how to rationally enhance enantioselectivities by means of proper tuning of the environment around the catalytic active site, and has resulted in the selection of Boc-*L*-tert-leucine as the preferred additive. Using these optimized conditions, manganese complex **2** was shown to be effective in the enantioselective benzylic oxidation of a series of arylalkane substrates with up to 50% alcohol yield and 62% product ee. A final set of experiments also highlights the use of the new 4-pyrrolidinopyridine-based complexes in the asymmetric epoxidation of olefins (up to 98% epoxide yield and >99% ee).

Received 9th September 2021,
Accepted 19th October 2021

DOI: 10.1039/d1cy01642c

rsc.li/catalysis

Introduction

The direct hydroxylation of C–H groups under catalytic conditions is an interesting strategy for late-stage functionalization.^{1–3} In biological systems, metallo-enzymes utilize dioxygen as terminal oxidant to perform such challenging transformations.⁴ Inspired by these systems, chemists have focused on the design of molecular catalysts making use of transition metals and using H₂O₂ as the terminal oxidant. Of special interest are enantioselective hydroxylation reactions due to the importance of chiral oxygenated molecules in natural products as well as in synthetic chemicals (agrochemicals, pharmaceuticals, etc.).

Several examples of enantioselective aliphatic C(sp³)–H oxidation catalysts exist, generally making use of manganese,

iron or ruthenium as the transition-metal, often in combination with porphyrin, salen or aminopyridine ligands.^{5–36} Among these systems, the ones based on manganese and iron supported by aminopyridine ligands have emerged as a very powerful family of catalysts.³⁷ It has been well established that such complexes activate H₂O₂, in most cases with the help of a carboxylic acid as an additive, to generate powerful and selective electrophilic metal-oxo species.^{22,23,38} On the one hand, the use of both non-heme iron and manganese complexes with aminopyridine ligands in asymmetric epoxidation reactions has been described extensively with high yields and enantioselectivities.^{39–62} On the other hand, the enantioselective oxidation of aliphatic C(sp³)–H bonds remains amongst the most challenging reactions, in which aminopyridine-based manganese complexes have particularly appeared as effective catalysts in the last years.⁶³

The general mechanism of this latter oxidation reaction entails an initial HAT step from the substrate to the high valent manganese-oxo species, followed by a hydroxyl rebound step to generate the final alcohol product. The main challenges are based on the stereoselection of the C–H bond oxidation, which usually originates from *enantio*-discriminating HAT (Fig. 1A) or OH rebound steps (Fig. 1B),³⁶

^a *Organic Chemistry and Catalysis, Debye Institute for Nanomaterials Science, Utrecht University, Universiteitsweg 99, 3584 CG Utrecht, The Netherlands.*
E-mail: r.j.m.kleingebink@uu.nl

^b *Structural Biochemistry, Bijvoet Centre for Biomolecular Research, Utrecht University, Universiteitsweg 99, 3584 CG Utrecht, The Netherlands*

† Electronic supplementary information (ESI) available: Experimental details, synthesis and characterization of ligands and complexes and selected GC and HPLC chromatograms. CCDC 2100950 and 2100951. For ESI and crystallographic data in CIF or other electronic format see DOI: 10.1039/d1cy01642c



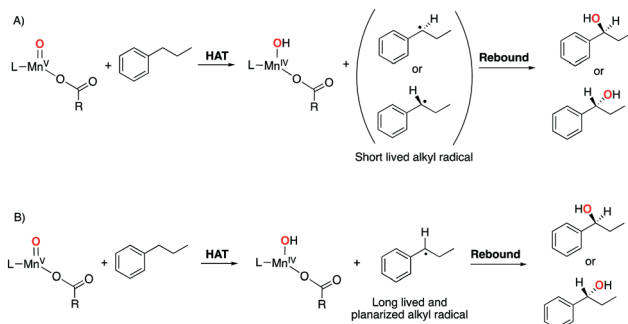


Fig. 1 Enantioselective aliphatic (benzylic) C–H oxidation of propylbenzene catalyzed by aminopyridine-based manganese complexes. A) Mechanism in which the origin of the enantioselectivity is determined at the HAT step.³⁶ B) Mechanism in which the origin of the enantioselectivity is determined at the rebound step (OH transfer step).³⁶

and the undesired overoxidation of the initial alcohol product producing ketone products. Regarding the latter drawback, a useful approach has been developed that makes use of hydrogen bond donor solvents, such as fluorinated alcohol solvents, to strongly deactivate electron rich C–H bonds that are in alpha-position to a hydroxyl group toward reaction with electrophilic reagents, thereby disfavoring alcohol overoxidation and preventing the loss of chirality. Accordingly, the use of fluorinated alcohol solvents has been

widely applied in different kinds of oxidation reactions.^{26,31,32,64–71}

Examples of enantioselective aliphatic C(sp³)–H oxidation reactions catalyzed by biologically inspired manganese complexes bearing aminopyridine ligands include a system to generate enantiomerically enriched products, that was reported by Bietti, Costas and co-workers. These authors developed a catalytic approach for the oxidative desymmetrization of mono-substituted cyclohexanes using bulky bioinspired manganese catalysts in combination with H₂O₂, generating γ -ketones with up to 85% yield and 96% ee.^{21,25} More recently, the enantioselective C–H lactonization of unactivated methylenes directed by carboxylic acids has also been described using the same kind of catalysts to afford chiral γ -lactones with up to 88% yield and >99% ee.³⁰ Focusing on enantioselective benzylic oxidation, Sun and co-workers developed an oxidative desymmetrization approach for the enantioselective oxidation of benzylic methylene groups of spirocyclic hydrocarbons by the bioinspired manganese catalyst **Mn(S-PEB)** and H₂O₂, affording up to 94% yield and 98% ee of the resulting ketone products (Fig. 2A).^{27,29} Later on, the same authors used their manganese-catalyzed system also for the oxidation of oxindoles and dihydroquinolinones, with up to 67% yield and 99% ee; as well as for the oxidation of benzylic methylene C–H bonds of indane-based substrates using

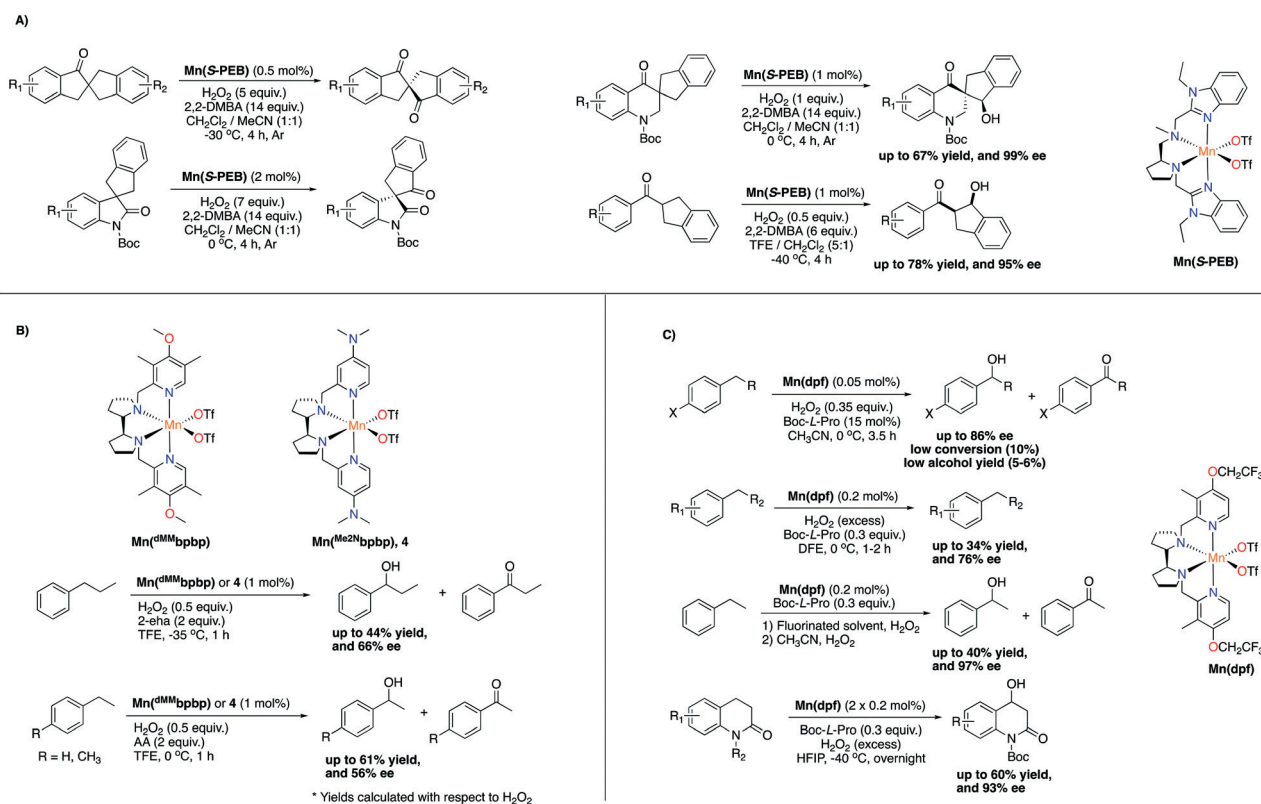


Fig. 2 Selected examples of enantioselective benzylic oxidation reactions catalyzed by aminopyridine-based manganese complexes (TFE = 2,2,2-trifluoroethanol, HFIP = 1,1,1,3,3,3-hexafluoro-2-propanol, AA = acetic acid, 2,2-DMBA = 2,2-dimethylbutanoic acid, 2-eha = 2-ethylhexanoic acid).



Complexation reactions were then performed by the reaction of equimolar amounts of the corresponding ligand with $[\text{Mn}^{\text{II}}(\text{CF}_3\text{SO}_3)_2]$ in dry THF under an inert atmosphere to afford manganese complexes (S,S) - $[\text{Mn}^{\text{II}}(\text{L1})(\text{CF}_3\text{SO}_3)_2]$ and (R,R) - $[\text{Mn}^{\text{II}}(\text{L1})(\text{CF}_3\text{SO}_3)_2]$ ((S,S) -**1** and (R,R) -**1**), and (S,S) - $[\text{Mn}^{\text{II}}(\text{L2})(\text{CF}_3\text{SO}_3)_2]$ (**2**) as microcrystalline solids (for further details see ESI†). Complexes (S,S) -**1** and **2** were characterized by high resolution mass spectrometry (HRMS). HRMS analysis of (S,S) -**1** showed a prominent mass peak at m/z 666.2378 corresponding to the $[\text{Mn}^{\text{II}}(\text{L1})(\text{CF}_3\text{SO}_3)_2]^+$ ion (calc. 666.2372). For complex **2** a prominent mass peak at m/z 664.2212 corresponding to the $[\text{Mn}^{\text{II}}(\text{L2})(\text{CF}_3\text{SO}_3)_2]^+$ ion (calc. 664.2215) was found. Manganese complexes (S,S) - $[\text{Mn}^{\text{II}}(\text{L3})(\text{CF}_3\text{SO}_3)_2]$ (**3**) and (S,S) - $[\text{Mn}^{\text{II}}(\text{L4})(\text{CF}_3\text{SO}_3)_2]$ (**4**) were also synthesized in order to compare the catalytic properties of the new complexes.^{43,49}

Synthesis of non-heme iron complex **5** was performed using equimolar amounts of **L2** and $[\text{Fe}^{\text{II}}(\text{CF}_3\text{SO}_3)_2(\text{CH}_3\text{CN})_2]$ in dry THF under an inert atmosphere. HRMS analysis of the complex showed a prominent mass peak at m/z 665.2189 corresponding to the $[\text{Fe}^{\text{II}}(\text{L2})(\text{CF}_3\text{SO}_3)_2]^+$ ion (calc. 665.2184).

Crystal and molecular structure of complexes **2** and **5**

The solid state structures and the enantiopurity of complexes **2** and **5** were confirmed by X-ray crystallography (Fig. 4).⁷⁹ Selected bond distances and bond angles for both complexes are listed in Table 1, and compared with the analogous manganese complex containing 4-dimethylaminopyridine moieties, (R,R) - $[\text{Mn}(\text{CF}_3\text{SO}_3)_2(\text{Me}_2\text{N}^i\text{bbpp})]$ ((R,R) -**4**).⁴³ The molecular structure of **2** shows that the manganese ion adopts a distorted octahedral coordination geometry with a *cis-α* conformation,⁸⁰ in which four coordination sites are occupied by nitrogen atoms of the tetradentate aminopyridine, while the remaining two sites are occupied by the oxygen atoms of the triflate anions in a *cis* orientation.

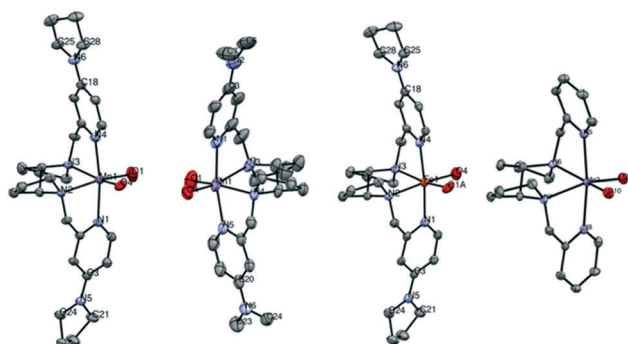


Fig. 4 From left to right: ORTEP diagrams of the molecular structure of (S,S) - $[\text{Mn}^{\text{II}}(\text{CF}_3\text{SO}_3)_2(\text{Pyr}^i\text{bbpp})]$ (**2**), (R,R) - $[\text{Mn}^{\text{II}}(\text{CF}_3\text{SO}_3)_2(\text{Me}_2\text{N}^i\text{bbpp})]$ ((R,R) -**4**), (S,S) - $[\text{Fe}^{\text{II}}(\text{CF}_3\text{SO}_3)_2(\text{Pyr}^i\text{bbpp})]$ (**5**), and (S,S) - $[\text{Mn}^{\text{II}}(\text{CF}_3\text{SO}_3)_2(\text{bbpp})]$ (**Mn(bbpp)**), showing the atom numbering scheme. Triflate anions are omitted except for the oxygen atoms directly bound to the metal center, and hydrogen atoms are omitted for clarity. The structure of complex (R,R) -**4** was reported by Costas and co-workers,⁴³ the structure of **Mn(bbpp)** by Bryliakov and co-workers.⁴⁰

The two pyridine moieties are placed above and below the plane containing the manganese center, whereas the two nitrogen of the (S,S) -bis-pyrrolidine backbone and the two oxygen atoms of the triflate ions are almost within the same plane, providing an overall C_2 -symmetric structure. In a similar way, the molecular structure of non-heme iron complex **5** shows a distorted octahedral coordination geometry with a *cis-α* conformation.

The Mn–N bond distances in complex **2** range from 2.222(3) to 2.300(3) Å and the Mn–O bond distances from 2.152(3) to 2.184(2) Å. These values compare quite well with the Mn–N and Mn–O bond distances of complex (R,R) -**4** (from 2.210(4) to 2.315(3) Å and 2.177(4) to 2.195(3) Å, respectively).⁴³ On the other hand, complex **2** displays a slightly smaller O–Mn–O angle (101.19(12)°) relative to the corresponding angle in complex (R,R) -**4** (104.08(14)°), which means that the 4-pyrrolidinopyridine moieties introduce some steric strain in the complex. The Fe–N bond distances in complex **5** range from 2.157(3) to 2.227(3) Å and the Fe–O bond distances are 2.153(3) Å, which are indicative of a high-spin iron complex.^{57,81} Comparing complexes **2** and **5**, we find that their structures are very much alike, with slightly longer Mn–N distances and similar Mn/Fe–O distances. The O–Fe–O angle of complex **5** is much smaller (94.01(11)°) than the O–Mn–O angle in **2** and (R,R) -**4** though, which we attribute to the difference in the ionic radius of the two metal ions (the ionic radius of Mn(II) being larger than that of Fe(II)). This observation is a general trend that has been observed for other iron and manganese complexes bearing the same ligand, such as for Mn and Fe complexes with the parent bbpp ligand (O–M–O angle of 107.45(9) and 85.81(5), respectively)^{40,82} and with the (S) -PEB ligand (see Fig. 2A for structure of the (S) -PEB ligand, O–M–O angle of 105.1(1) and 101.5(2), respectively).^{83,84}

Overall, the molecular structure of complexes **2** and **5** do not differ significantly from the structure of 4-dimethylamino-substituted complex (R,R) -**4**, nor from the non-substituted bis-pyrrolidine manganese complex (**Mn(bbpp)**).⁴⁰ This shows that the pyrrolidine and dimethylamino substituents provide similar structural properties to the complexes. Accordingly, the introduction of a pyrrolidine substituent in the *para*-position of each pyridine ring of the bbpp ligand does not produce significant changes in the structural geometry of the complex.

Pyrrolidine vs. dimethylamino: amine-substituted pyridines in Mn-catalyzed benzylic oxidation

We rationalize that 4-pyrrolidinopyridine is a stronger *N*-heteroaromatic electron donor moiety compared to DMAP and pyridine ($pK_a = 18.33$, 17.95 and 12.53 for 4-pyrrolidinopyridine, DMAP and pyridine, respectively),^{77,78} and accordingly we believe that complex (S,S) -**1** and **2**, containing the tetradentate aminopyridine ligands with the pyrrolidine substituents, will better stabilize the active oxidant that is being formed upon reaction of the complex



Table 1 Selected bond lengths (Å) and angles (°) for manganese complexes **2**, (*R,R*)-**4**, **5** and Mn(**bbpp**)⁴⁰

2		<i>(R,R)</i> - 4 (ref. 43)		5		Mn(bbpp) ⁴⁰	
Mn1–N1	2.222(3)	Mn1–N1	2.210(4)	Fe1–N1	2.157(3)	Mn2–N8	2.250(2)
Mn1–N4	2.215(3)	Mn1–N5	2.210(3)	Fe1–N4	2.162(3)	Mn2–N5	2.239(2)
Mn1–N2	2.294(3)	Mn1–N3	2.301(4)	Fe1–N2	2.226(3)	Mn2–N7	2.273(2)
Mn1–N3	2.300(3)	Mn1–N4	2.315(3)	Fe1–N3	2.227(3)	Mn2–N6	2.300(2)
Mn1–O1	2.152(3)	Mn1–O1	2.177(4)	Fe1–O4	2.153(3)	Mn2–O7	2.145(2)
Mn1–O4	2.184(2)	Mn1–O4	2.195(3)	Fe1–O1	2.153(3)	Mn2–O10	2.152(2)
N6–C25	1.474(5)	N2–C6	1.450(6)	N6–C28	1.472(5)	—	—
N6–C28	1.462(5)	N2–C7	1.457(8)	N6–C25	1.463(5)	—	—
N6–C18	1.346(4)	N2–C3	1.344(7)	N6–C18	1.346(5)	—	—
N5–C24	1.466(4)	N6–C24	1.434(6)	N5–C24	1.462(5)	—	—
N5–C21	1.466(5)	N6–C23	1.469(6)	N5–C21	1.470(5)	—	—
N5–C3	1.346(4)	N6–C20	1.352(5)	N5–C3	1.348(5)	—	—
N1–Mn1–N2	76.26(10)	N4–Mn1–N5	75.45(11)	N1–Fe1–N2	77.76(11)	N8–Mn2–N7	74.80(8)
N3–Mn1–N4	75.87(10)	N3–Mn1–N1	74.80(13)	N3–Fe1–N4	77.37(11)	N6–Mn2–N5	76.03(9)
N2–Mn1–N3	77.11(10)	N3–Mn1–N4	77.25(12)	N2–Fe1–N3	79.40(10)	N7–Mn2–N6	78.68(9)
N2–Mn1–N4	95.53(10)	N1–Mn1–N4	91.89(12)	N2–Fe1–N4	96.48(11)	N7–Mn2–N5	101.02(9)
O1–Mn1–O4	101.19(12)	O1–Mn1–O4	104.08(14)	O4–Fe1–O1	94.01(11)	O7–Mn2–O10	103.52(8)
C25–N6–C28	112.3(3)	C6–N2–C7	117.2(5)	C28–N6–C25	111.7(3)	—	—
C18–N6–C28	124.0(3)	C3–N2–C7	120.7(4)	C18–N6–C25	124.5(3)	—	—
C21–N5–C24	112.3(3)	C23–N6–C24	117.7(4)	C21–N5–C24	112.2(3)	—	—
C3–N5–C21	124.1(3)	C20–N6–C23	120.4(4)	C3–N5–C21	124.5(3)	—	—

with H₂O₂, that is the high-valent manganese-oxo species.^{29,37,38,63,85–87} Thus, we have tested manganese complexes (*S,S*)-**1** and **2** (1 mol%) in catalytic benzylic oxidation reactions in the presence of acetic acid as additive and 2,2,2-trifluoroethanol (TFE) as solvent, using propylbenzene (**6**, 0.2 mmol) as model substrate (Table 2). For comparison purposes, manganese complexes **3** and **4** were also tested for the same oxidation reaction. Aqueous hydrogen peroxide (1 equiv.) was delivered at –35 °C over a period of 30 min using a syringe pump (see ESI† for further details on catalytic conditions). Crude mixtures were analyzed by GC to screen for benzylic oxidization products. The benzylic alcohol product **6a** was detected as the main oxidized product, together with the overoxidized ketone **6b** as a minor product, indicating that the first-formed alcohol product can engage in a second oxidation step even in the

presence of a fluorinated alcohol solvent. Products deriving from oxidation at the aromatic ring (*para*-phenol, *ortho*-phenol and benzoquinone) were also detected in small amounts, indicating that aromatic oxidation takes place to a small extent using the current manganese complexes. This finding agrees with our previous study on the oxidation of aromatic substrates catalyzed by bioinspired manganese complexes, where electron-rich Mn complexes show the formation of benzylic alcohols as the main oxidized product, whereas aromatic oxidation toward phenols occurs to a lower extent.⁷³

Under these conditions, complexes (*S,S*)-**1** and **2** generate the alcohol product **6a** in 34 to 35% yield, together with the ketone product **6b** in 4 to 5% yield and trace amounts of the aromatic oxidation products. For both complexes the (*S*)-alcohol product formed in 32 and 33% ee, respectively,

Table 2 Catalytic enantioselective benzylic oxidation of propylbenzene (**6**) with AA

Catalyst	r.s.m ^a	Alcohol ^b	Ketone ^b	<i>p</i> -Phenol ^b	<i>o</i> -Phenol ^b	Quinone ^b	ee ^c	MB ^d
(<i>S,S</i>)- 1	26	35	4	1	<1	1	32	68
2	34	34	5	<1	n.d.	1	33	74
3	43	23	1	2	1	1	39	71
4	37	27	4	1	<1	1	36	70
5	25	<1	n.d.	<1	<1	<1	—	25

^a Remaining starting material (r.s.m) in %. ^b Yields in % with respect to substrate determined by GC against an internal standard.

^c Enantiomeric excess determined by HPLC on a chiral stationary phase. (*S*)-(-)-1-Phenyl-1-propanol (**6a**) was obtained as the major enantiomer.

^d Mass balance (MB) was calculated considering remaining starting material and all products formed: MB = (r.s.m%) + (Product Yields%). n.d. = non-detected. AA = acetic acid.



showing that a change in the amine backbone does not induce a significant change in enantioselectivity. Complexes **3** and **4** yield the benzylic alcohol product **6a** in 23 and 27%, respectively, in this reaction, whereas the ketone yield is low (1% and 4%, respectively). The ee value for the (*S*)-alcohol obtained for these latter manganese complexes ranges between 36% and 39%, showing a slight increase compared to complexes (*S,S*)-**1** and **2**. Overall, when acetic acid is used as additive, complexes (*S,S*)-**1** and **2** afford a higher catalytic activity than complexes **3** and **4** based on substrate conversion and combined alcohol and ketone yield, whereas ee values are slightly lower. Mass balances of these reactions are not excellent, which could indicate that overoxidation to non-detected products may occur.

Worthy of note is that use of non-heme iron complex **5** in this reaction resulted in the formation of only trace amounts of benzylic alcohol product **6a**, while substrate conversion was considerable (75%), indicating a poor mass balance for this reaction. This observation indicates that the use of iron as the metal is not optimal for this aliphatic (benzylic) hydroxylation reaction. Moreover, *para*-phenol, *ortho*-phenol and quinone products were also detected in trace amounts, indicating that complex **5** shows aromatic oxidation to some extent, which was also noted by Bryliakov and co-workers for related non-heme iron complexes supported by tetradentate aminopyridine ligands.^{88–91} Accordingly, we focused our study on benzylic oxidation exclusively on the use of manganese complexes as catalysts.

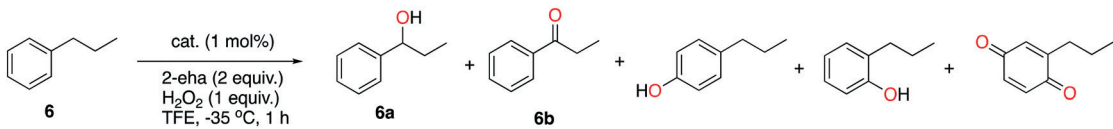
Because of the importance of carboxylic acids in H₂O₂-mediated oxidation catalysis, we decided to investigate different carboxylic acid additives. One of the carboxylic acids that has shown promising results in aliphatic C–H hydroxylation, as well as in epoxidation reactions, is racemic 2-ethylhexanoic acid (2-eha). When using this acid, an increase in ee values of the alcohol product has been documented for several manganese-catalyzed and iron-catalyzed oxidations.^{42,43,45,57,59,92} Therefore, here we have studied the oxidation of substrate **6** using 2-eha following the previously mentioned conditions (Table 3).

With 2-eha, complexes (*S,S*)-**1** and **2** showed similar benzylic alcohol yields as with the use of acetic acid (34% yield), whereas the formation of overoxidized ketone product slightly increased to 7–8% yield. Interestingly, ee values for the alcohol product increase for all complexes when 2-eha is employed. Complexes (*S,S*)-**1** and **2** showed ee values for the (*S*)-alcohol product up to 59%, which means a two-fold increase in comparison with the use of acetic acid as additive (compare Tables 2 and 3). For the manganese complexes bearing 4-dimethylaminopyridine groups (**3** and **4**), the ee value increased in a similar way only in the case of complex **3** containing the bis-pyrrolidine backbone (58% ee), whereas complex **4** based on the *N,N*-cyclohexanediamine backbone showed a smaller increase (50% ee). Also under these conditions, complexes **3** and **4** showed lower conversions and alcohol and ketone yields compared to complexes (*S,S*)-**1** and **2**.

From these results, we concluded that manganese complexes (*S,S*)-**1** and **2** with either a bis-pyrrolidine or a *N,N*-cyclohexanediamine backbone are promising catalysts for benzylic oxidations, since they show high ee values for the alcohol product. Comparing our results to the systems previously described by Costas⁶⁸ and Bryliakov,^{24,26,32,72} we can conclude that the current complexes perform the benzylic hydroxylation of an alkylbenzene with ee's commensurate to state-of-the-art homogeneous catalysts (see Fig. 2B and C). In addition, complexes (*S,S*)-**1** and **2** show higher conversions and benzylic alcohol yields (34% yield) than complexes **3** and **4** bearing 4-dimethylaminopyridine moieties. We believe that the reason for the (slight) increase in alcohol yield is caused by the higher basicity of the ligands resulting from the pyrrolidine substituents, which provide the complex with a more electron-donating ligand and therefore might provide a better stabilization of the active oxidant.

Complex **2** was then chosen for further reaction optimization, since a better mass balance was observed compared to the use of complex (*S,S*)-**1**. Initially the use of another fluorinated solvent, *i.e.* 1,1,1,3,3,3-hexafluoro-2-

Table 3 Catalytic enantioselective benzylic oxidation of propylbenzene with 2-eha



Catalyst	r.s.m. ^a	Alcohol ^b	Ketone ^b	<i>p</i> -Phenol ^b	<i>o</i> -Phenol ^b	Quinone ^b	ee ^c	MB ^d
(<i>S,S</i>)- 1	31	34	7	<1	1	n.d.	59	73
2	39	34	8	n.d.	n.d.	n.d.	58	81
3	44	26	3	<1	<1	n.d.	50	73
4	38	30	6	n.d.	n.d.	n.d.	58	74

^a Remaining starting material (r.s.m) in %. ^b Yields in % with respect to substrate determined by GC against an internal standard.

^c Enantiomeric excess determined by HPLC on a chiral stationary phase. (*S*)-(-)-1-Phenyl-1-propanol (**6a**) was obtained as the main enantiomer.

^d Mass balance (MB) was calculated considering remaining starting material and all products formed: MB = (r.s.m%) + (Product Yields%). n.d. = non-detected. 2-eha = 2-ethylhexanoic acid.



propanol (HFIP), was explored using acetic acid and 2-eha as additives (see Table S1†). In these experiments, a high alcohol/ketone product ratio (A/K of 31 and 18, using AA and 2-eha, respectively) was observed with only trace amounts of overoxidized ketone product being formed. This observation agrees with the stronger hydrogen bond donor ability of HFIP compared with TFE (A/K = 4.25 for complex 2 in combination with 2-eha in TFE), providing an enhanced polarity reversal to alcohol groups and favoring the deactivation of proximal C–H bonds toward oxidation by high valent metal-oxo species.⁶⁸ However, due to the higher melting point of HFIP compared to TFE (−3.3 and −43.5 °C, respectively), the reaction in HFIP was performed at a higher reaction temperature of 0 °C, resulting in lower ee values of the alcohol product when 2-eha was employed (48% and 58% for HFIP and TFE, respectively). Using acetonitrile as the solvent in the current oxidation reaction provided a low alcohol/ketone ratio (A/K of 0.2 and 0.5, using AA and 2-eha, respectively), indicating that overoxidation of the primary alcohol product is highly favored in this solvent (see Table S1†). Thus, TFE was chosen as the solvent for further reaction optimization, because it provides good A/K product ratios and allows the reaction to be performed at a lower temperature (−35 °C), which has been shown to be crucial to obtain good enantioselectivities.

Carboxylic acid optimization

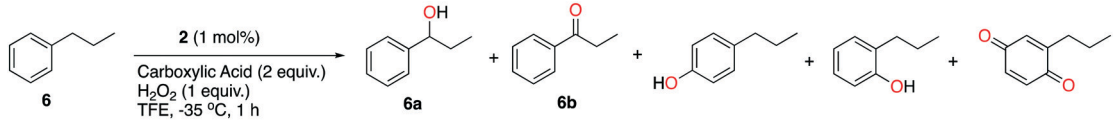
Since our data showed that the enantioselectivity of the manganese-catalyzed benzylic oxidation reaction changes upon variation of the carboxylic acid additive, we decided to look in more detail into different types of acids. It is well known that these H₂O₂-mediated aliphatic oxidation reactions proceed through a so-called “carboxylic acid-assisted” pathway, in which the acid is bound to the active oxidant after O–O bond cleavage of a manganese–hydroperoxo intermediate to form a high-valent manganese-oxo species.^{38,42,85,93,94} On basis of this mechanism, we believe that choosing a carboxylic acid with the optimal structure might be a key factor to engineer a proper chiral

environment around the catalytic site to generate an oxidant capable of performing benzylic oxidations with high levels of enantioselectivity. Accordingly, we have screened several carboxylic acid additives for their impact on overall catalytic activity and more specifically on product enantioselectivity (Fig. S1† shows the structures of the carboxylic acids used in this study).

First, we decided to test a series of carboxylic acids with different types of alpha-carbons. We have considered an acid with a primary alpha-carbon (acetic acid, AA), a secondary (propionic acid, PA), a tertiary (2-ethylhexanoic acid, 2-eha), a quaternary (2,2-dimethylbutanoic acid, 2,2-DMBA), as well as an sp²-hybridized alpha-carbon (benzoic acid, BZA). Table 4 summarizes the catalytic data for the use of this set of additives in the oxidation of propylbenzene (6). Increasing the length of the alkyl chain of the carboxylic acid, by using propionic acid, did provide a slight increase in alcohol and ketone yield (38% and 7% yield, respectively) compared to the use of AA. However, the ee value for the alcohol product did not increase (Table 4, entry 1 and 2). Interestingly, when acids with tertiary and quaternary alpha-carbons were used (2-eha and 2,2-DMBA), ee values for the benzylic alcohol significantly increased (58% ee), without deterioration of the alcohol yield (Table 4, entry 3 and 4). Worthy of note is the use of 2,2-DMBA, which provided a significant increase in ketone formation (14% yield), clearly favoring oxidation of the initial alcohol product compared to the other carboxylic acids tested. The use of this acid does also provide the alcohol with an increased ee. The use of a carboxylic acid with an sp²-hybridized alpha-carbon, such as benzoic acid, resulted in a decrease in alcohol ee (25% ee) compared to the use of AA, as well as in a lower alcohol yield (Table 4, entry 5). Accordingly, this first data set indicated that the use of a carboxylic acid additive with a tertiary sp³-hybridized alpha-carbon provides the best results in terms of alcohol yield and ee value. In all these cases, aromatic oxidation is basically suppressed to a minimum.

Next, we decided to screen a set of carboxylic acids with tertiary alpha-carbons in which the substitution on one of

Table 4 Screening of carboxylic acids with different types of alpha-carbons



Entry	CA ^a	r.s.m. ^b	Alcohol ^c	Ketone ^c	<i>p</i> -Phenol ^c	<i>o</i> -Phenol ^c	Quinone ^c	ee ^d	MB ^e
1	AA	34	34	5	<1	n.d.	1	33	74
2	PA	29	38	7	1	n.d.	n.d.	34	75
3	2-eha	39	34	8	n.d.	n.d.	n.d.	58	81
4	2,2-DMBA	31	27	14	n.d.	n.d.	n.d.	58	72
5	BZA	37	23	7	n.d.	n.d.	n.d.	25	67

^a Carboxylic acid: AA = acetic acid, PA = propionic acid, 2-eha = 2-ethylhexanoic acid, 2,2-DMBA = 2,2-dimethylbutanoic acid, BZA = benzoic acid.

^b Remaining starting material (r.s.m) in %. ^c Yields in % with respect to substrate determined by GC against an internal standard.

^d Enantiomeric excess determined by HPLC on a chiral stationary phase. (*S*)-(-)-1-Phenyl-1-propanol (6a) was obtained as the main enantiomer.

^e Mass balance (MB) was calculated considering remaining starting material and all products formed: MB = (r.s.m%) + (Product Yields%). n.d. = non-detected.



the beta-carbons varies (see ESI,† Table S2). On basis of this analysis, we concluded that an acid additive containing a tertiary alpha-carbon and a secondary beta-carbon (such as 2-cha) provides the best performance in the H₂O₂-mediated benzylic oxidation of propylbenzene with manganese catalyst 2. Interestingly, using this set of carboxylic acid additives led to a complete suppression of aromatic oxidation activity.

Finally, we considered the use of chiral amino acids as carboxylic acid additives. Recent studies have shown the advantageous use of these additives in other H₂O₂-mediated oxidations using bioinspired manganese complexes as catalysts.^{24,26,32,72} Amino acids comprise a tertiary alpha-carbon, which seems optimal for enantioselective benzylic oxidation with catalyst 2 on the basis of our screening of carboxylic acids with different types of alpha-carbons (Table 4). Accordingly, we have tested *N*-protected prolines, leucines and phenylalanines containing different protecting groups (Boc, Cbz and Phth) and chiralities (*L* and *D*) (Table 5).

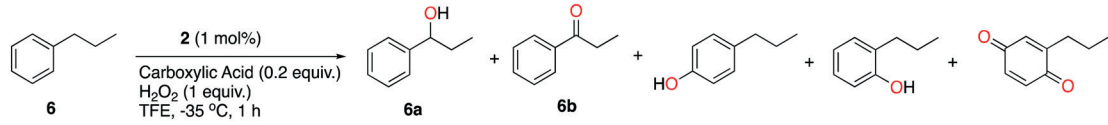
Regarding the prolines employed, we have considered both Boc-*L*-proline and a Cbz-*L*-proline. For Boc-*L*-proline we obtained up to 31% alcohol yield in 47% ee and 7% ketone yield, (Table 6, entry 1). For Cbz-*L*-proline we obtained a higher conversion and yields, with the alcohol product being formed in 38% yield, and the ketone in 6% yield. The ee value for the alcohol product in this case was 52%. Since the Cbz protecting group provided better conversion and yields, we decided to also test the Cbz-proline additive with opposite stereochemistry *D* (Table 6, compare entries 2 and 3). Interestingly, we found that the overall activity of the current system changes by switching the chirality of the amino acid additive, indicating that a proper engineering of the chiral environment around the catalytic active site is crucial, and that subtle modifications may translate into different performances. The experiment using Cbz-*D*-Pro provided a lower conversion and alcohol yield, whereas the alcohol ee increased to 61% (Table 6, entry 3). Next, we have also considered leucines with different chiralities (Boc-*L*-*tert*-leucine and Boc-*D*-*tert*-leucine) as amino acid additives. Boc-*L*-

tert-leucine provides the benzylic alcohol product in up to 42% yield, together with the ketone product in 9% yield. The ee value in this case was as high as 58%. The use of the opposite enantiomer, Boc-*D*-*tert*-leucine, again led to a different catalytic performance. The yield for the alcohol product decreased to 30%, whereas the ketone product was formed in a much higher amount (16%). The ee value for the alcohol product slightly decreased to 52%. Finally, we have also considered phthalamido-protected *L*-phenylalanine as additive. However, product yields were much lower with only 24% alcohol yield and 5% ketone yield, and an ee value of 46% was observed for the alcohol product (Table 6, entry 6).

An important observation from these experiments is that by switching the chirality of the amino acid additive, the enantioselectivity in the alcohol product does not change for this catalytic system, *i.e.* the (*S*)-alcohol is observed as the major product in all cases. Therefore, we can conclude that the enantioselectivity of the reaction is dictated by the chirality of the starting Mn-complex and is not perturbed by (chiral) additives, as was previously described in other studies using similar manganese complexes for the oxidation of aliphatic C–H bonds.^{26,32} Indeed, by using complex (*S,S*)-1 in combination with 2-cha, the (*S*)-(-)-1-phenyl-1-propanol product was generated as the main enantiomer in 59% ee, while the (*R*)-(+)-1-phenyl-1-propanol product formed as the main enantiomer in 57% ee at a similar conversion and yield when using complex (*R,R*)-1 of opposite chirality (see ESI,† Table S3).

From the data compiled in Table 6, we concluded that the best carboxylic acid additive is Boc-*L*-*tert*-leucine, providing the highest benzylic alcohol yield (42%) and a good ee value (58%). These characteristics could be slightly increased by making use of an iterative addition protocol (see ESI,† for further details). This methodology consists of adding a first portion of manganese complex (0.5 mol%) and carboxylic acid additive (0.2 equiv.) and adding H₂O₂ (0.5 equiv.) over a period of 1 h. Then, a new portion of complex (0.5 mol%) and carboxylic acid (0.2 equiv.) is added, and a second

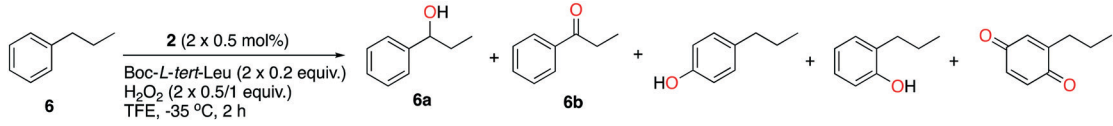
Table 5 Screening of *N*-protected amino acids as carboxylic acid additives containing tertiary alpha-carbons



Entry	CA ^a	r.s.m ^b	Alcohol ^c	Ketone ^c	<i>p</i> -Phenol ^c	<i>o</i> -Phenol ^c	Quinone ^c	ee ^d	MB ^e
1	Boc- <i>L</i> -Pro	46	31	7	<1	n.d.	n.d.	47	84
2	Cbz- <i>L</i> -Pro	27	38	6	1	n.d.	n.d.	52	72
3	Cbz- <i>D</i> -Pro	39	27	4	1	n.d.	n.d.	61	71
4	Boc- <i>L</i> - <i>tert</i> -Leu	29	42	9	<1	n.d.	n.d.	58	80
5	Boc- <i>D</i> - <i>tert</i> -Leu	37	30	16	n.d.	n.d.	n.d.	52	83
6	Phth- <i>L</i> -Phe	43	24	5	<1	n.d.	n.d.	46	72

^a Carboxylic acid: Boc-*L*-Pro = *N*-*tert*-butylcarboxy-*L*-proline, Cbz-*L*-Pro = *N*-carbobenzyloxy-*L*-proline, Cbz-*D*-Pro = *N*-carbobenzyloxy-*D*-proline, Boc-*L*-*tert*-Leu = *N*-*tert*-butylcarboxy-*L*-leucine, Boc-*D*-*tert*-Leu = *N*-*tert*-butylcarboxy-*D*-leucine, Phth-*L*-Phe = phthalamido-*L*-phenylalanine. ^b Remaining starting material (r.s.m) in %. ^c Yields in % with respect to substrate determined by GC against an internal standard. ^d Enantiomeric excess determined by HPLC on a chiral stationary phase. (*S*)-(-)-1-Phenyl-1-propanol (6a) was obtained as the main enantiomer. ^e Mass balance (MB) was calculated considering remaining starting material and all products formed: MB = (r.s.m%) + (Product Yields%). n.d. = non-detected.



Table 6 Iterative addition protocol for the oxidation of propylbenzene using complex **2** and Boc-L-tert-Leu as the additive


Entry	H ₂ O ₂ ^a	r.s.m ^b	Alcohol ^c	Ketone ^c	<i>p</i> -Phenol ^c	<i>o</i> -Phenol ^c	Quinone ^c	ee ^d	MB ^e
1	2 × 0.5	23	46	9	n.d.	n.d.	n.d.	60	78
2	2 × 1	<1	23	55	<1	n.d.	n.d.	72	78

^a Total equivalents of H₂O₂ used in the oxidation reaction (added in two portions). ^b Remaining starting material (r.s.m) in %. ^c Yields in % with respect to substrate determined by GC against an internal standard. ^d Enantiomeric excess determined by HPLC on a chiral stationary phase. (S)-(-)-1-Phenyl-1-propanol (**6a**) was obtained as the main enantiomer. ^e Mass balance (MB) was calculated considering remaining starting material and all products formed: MB = (r.s.m%) + (Product Yields%). n.d. = non-detected.

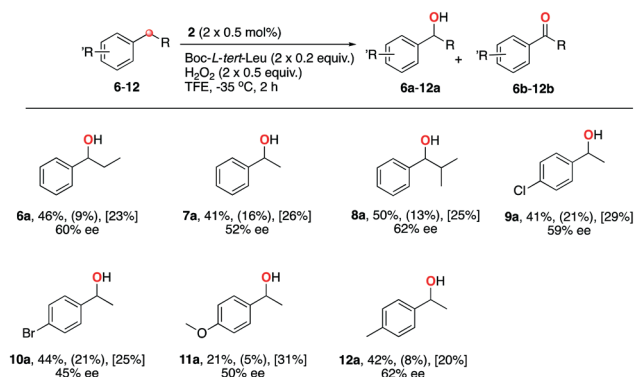
portion of H₂O₂ (0.5 equiv.) is added again over a period of 1 h. This procedure provided us with a slight increase in conversion and alcohol yield (up to 46%), keeping a similar ee value of 60% (Table 7, entry 1). This observation could indicate that catalyst lifetime is an issue in these H₂O₂-mediated C–H oxidations, as it has been previously described that oxidative degradation of the ligand occurs for related non-heme iron and manganese complexes.^{95–97} When the same iterative addition protocol was used but employing a total of 2 equiv. of H₂O₂, the overoxidized ketone product was obtained as the main product in 55% yield, together with the alcohol product in 23% yield, indicating that overoxidation is highly favored when a large excess of oxidant is used (Table 7, entry 2). Interestingly, the ee value for the alcohol product increased to 72%, which can be explained by a kinetic resolution effect in the secondary oxidation step. This kinetic resolution methodology has been previously used to reach high alcohol ee values by Bryliakov *et al.*^{24,32,98} The iterative addition protocol using an overall 2.0 equiv. of oxidant also led to full substrate conversion. Overall, the catalytic system 2/H₂O₂/Boc-L-tert-leucine performs the oxidation of monoalkylbenzene **6** with higher alcohol yields compared to the system developed by Bryliakov and co-workers.²⁶ Similar conversions were obtained for both systems (~75%), whereas alcohol yield was higher with the current complex (46% and 34% alcohol yield for the use of catalyst **2** and **Mn(dpf)**, respectively). However, ee values for the alcohol product were lower when **2** was used instead of **Mn(dpf)** (60% and 76% ee for the use of catalyst **2** and **Mn(dpf)**, respectively). Of note is that ee's have been considerably increased using a kinetic resolution approach with **Mn(dpf)**, obtaining up to 97% alcohol ee (Fig. 2C).³²

Substrate scope

Using the optimized reaction conditions, including Boc-L-tert-leucine as the carboxylic acid additive, we explored the enantioselective benzylic hydroxylation of different aromatic substrates by manganese complex **2** (Scheme 1). In general, our current catalytic system with the highly electron-rich manganese complex and an enantiopure amino acid additive

affords a high selectivity for aliphatic (benzylic) C–H bond oxidation over aromatic oxidation of these substrates.

Oxidation of ethylbenzene (**7**) leads to the benzylic alcohol product **7a** in 41% yield and 52% ee, along with the corresponding ketone **7b** in 16% yield. Interestingly, isobutylbenzene (**8**) was also considered, which bears a reactive tertiary aliphatic C–H bond. Benzylic alcohol product **8a** was obtained in 50% yield and 62% ee, together with the corresponding ketone product **8b** in 13% yield. The 2-methyl-1-phenyl-2-propanol product derived from oxidation at the tertiary position was only detected in trace amounts, which agrees with the favorable oxidation of a benzylic C–H bond (activated C–H bond, BDE = 85.4 kcal mol⁻¹) compared to a tertiary aliphatic C–H bond (non-activated C–H bond, BDE = 96 kcal mol⁻¹).⁹⁹ Next, we extended our study to the oxidation of *para*-substituted ethylbenzenes as substrates, containing electron-withdrawing and electron-donating substituents. Oxidized products were obtained in good benzylic alcohol yields ranging from 21 to 50%, with overoxidized ketone products between 5 and 21% yield. Enantioselectivity values



Scheme 1 Asymmetric synthesis of benzylic alcohols by a manganese-catalyzed C–H oxidation. Reactions were performed on 0.2 mmol scale in 2.5 mL of TFE, 0.5 mol% of complex **2** and 0.2 equiv. of Boc-L-tert-Leu (complex **2**, carboxylic acid, and oxidant were all added in portionwise twice; for details, see the ESI[†]). Yields were determined by GC, and ee was determined by HPLC on a chiral stationary phase. Yields for the overoxidized ketone products are shown in parenthesis, whereas remaining starting material (r.s.m%) is shown in brackets.



Table 7 Catalytic asymmetric epoxidation of *cis*- β -methylstyrene with manganese complexes

Entry	Catalyst	CA ^a	r.s.m. ^b	Epoxide ^c	ee ^d
1	(<i>S,S</i>)-1	AA	<1	98	78
2	(<i>S,S</i>)-1	2-eha	<1	98	93
3	2	AA	<1	98	84
4	2	2-eha	<1	98	97

^a Carboxylic acid: AA = acetic acid, 2-eha = 2-ethylhexanoic acid. ^b Remaining starting material (r.s.m) in %. ^c Yields in % with respect to substrate determined by GC against an internal standard. ^d Enantiomeric excess determined by chiral GC.

for the alcohol product range from 45 to 62%. Oxidation of 1-chloro-4-ethylbenzene (**9**), containing an electron-withdrawing substituent, provided the alcohol product **9a** in 41% yield and 59% ee, together with ketone byproduct **9b** in 21% yield. 1-Bromo-4-ethylbenzene (**10**) was also considered, which yielded the desired benzylic alcohol product **10a** in 44% yield and 45% ee, generating the ketone product **10b** in 21% yield. Oxidation of 4-ethylanisole (**11**), which bears an electron-donating substituent, provided lower activities, with the benzylic alcohol product **11a** in 21% yield and 50% ee, with the ketone **11b** being formed in only 5% yield. A dialkylbenzene was also considered in the current work. Particularly, we explored the oxidation of 4-ethyltoluene (**12**), which contains two benzylic positions. Interestingly, reaction mainly occurred on the ethyl substituent, which bears the C–H bonds with the lower BDE (85.4 and 89.7 kcal mol⁻¹ for the BDE of the benzylic C–H bond of ethylbenzene and toluene, respectively),⁹⁹ affording the benzylic alcohol product **12a** in 42% yield and 62% ee, with the ketone product **12b** in 10% yield. Oxidation at the other benzylic position occurred to a much lower extent, generating 4-ethylbenzyl alcohol in 5% yield. Other by-products were also detected, which might be assigned to products in which oxidation takes place at both alkyl substituents.

Asymmetric epoxidation reactions

Finally, to provide an extended impression of their catalytic properties, the new manganese complexes (*S,S*)-1 and 2 were also tested in the epoxidation reaction of *cis*- β -methylstyrene (**13**) as substrate (Table 7). The outcome of these experiments shows that these complexes are highly efficient epoxidation catalysts as well, with yields up to 98% for the epoxide product **13a** using only 1 equiv. of the H₂O₂ oxidant, and up to 97% ee for the epoxide product when 2-eha is employed as carboxylic acid additive. The use of 2-eha as the carboxylic acid additive instead of acetic acid leads to a significant increase in enantioselectivity, as was reported before for related non-heme iron and manganese complexes.⁴² 2-Cyclohexene-1-one (**14**) represents a much more challenging, electron-poor substrate for epoxidation reactions. Using manganese catalysts (*S,S*)-1 and 2, the epoxide product **14a** was obtained in poor yields, with values up to 28 and 19%, respectively, when acetic acid was used as additive (Table 8, entries 1 and 3). Changing the carboxylic acid to 2-eha provided a significant decrease in epoxide yield (Table 8, entries 2 and 4).

For these reactions we have not been able to determine the enantioselectivity due to low concentration of the epoxide

Table 8 Catalytic asymmetric epoxidation of 2-cyclohexene-1-one using manganese and iron complexes

Entry	Catalyst	CA ^a	r.s.m. ^b	Epoxide ^c	ee ^d
1	(<i>S,S</i>)-1	AA	24	28	—
2	(<i>S,S</i>)-1	2-eha	57	4	—
3	2	AA	35	19	—
4	2	2-eha	48	10	—
5	5	AA	13	67	53
6	5	2-eha	20	56	>99

^a Carboxylic acid: AA = acetic acid, 2-eha = 2-ethylhexanoic acid. ^b Remaining starting material (r.s.m) in %. ^c Yields in % with respect to substrate determined by GC against an internal standard. ^d Enantiomeric excess determined by HPLC on a chiral stationary phase. Ee values for Mn-catalyzed oxidations were not possible to determine due to low epoxide formation.



product. Next, we tested the non-heme iron complex **5**, which provided much higher efficiencies for the epoxidation of **14**, with yields up to 67 and 56% when acetic acid and 2-eha were employed, respectively. This observation contrasts with the previous study on enantioselective benzylic oxidations, where catalyst **5** was not capable of performing the aliphatic C–H hydroxylation of propylbenzene towards the benzylic alcohol product, and it shows that a highly electron-rich iron complex performs better for the epoxidation of aliphatic olefins compared to the analogous manganese complexes. Remarkably, the enantioselectivity obtained when **5** is used in the presence of 2-eha was excellent (>99%), which represents an increase compared with the related non-heme iron complex supported with the aminopyridine ligand containing dimethylamino substituents.⁵⁹

Overall, the current complexes containing 4-pyrrolidinopyridine moieties provide enhanced enantioselectivities for the epoxidation of olefins. This finding is in accordance with the increase in enantioselectivity reported in previous studies by the introduction of dimethylamino or other similar amine substituents into several manganese and iron complexes, compared to the use of complexes with non-substituted pyridines.^{37,43,45,49,52,53,61}

Conclusions

A new series of chiral manganese and iron complexes supported by highly electron-donating pyridylalkylamine ligands containing 4-pyrrolidinopyridine moieties ((*S,S*)-**1**, (*R,R*)-**1**, **2** and **5**) were synthesized and characterized. The manganese complexes were tested as efficient catalysts for enantioselective benzylic oxidations using H₂O₂ as terminal oxidant in the presence of fluorinated alcohol solvents and carboxylic acid additives for the controlled activation of H₂O₂. The current complexes afford improved benzylic alcohol yields compared with the analogous manganese complexes with 4-dimethylaminopyridine moieties (**3** and **4**), which we rationally assign to the higher basicity of the 4-pyrrolidinopyridine group. In addition, we have presented a systematic study on the modulation of the carboxylic acid additive for the proper engineering of the environment around the catalytic active site, which has allowed the formation of several benzylic alcohol products in moderate to good enantioselectivities. Finally, we have also shown that the current manganese and iron complexes are effective catalysts for the asymmetric epoxidation of olefins at low oxidant loadings, with special emphasis on the good yields and excellent enantioselectivities obtained for the epoxidation of a challenging olefin catalyzed by non-heme iron complex **5**.

Future efforts in our laboratory will focus on the further development of highly electron-rich manganese and iron complexes that make use of strong electron-donating ligands for a better stabilization of the metal-oxo active species. Improvement of enantioselectivities for benzylic alcohol products, as well as the understanding of the factors that

govern product chemoselectivity (aliphatic vs. aromatic oxidation) are currently being explored.

Author contributions

E. M. and R. K. G. devised the project and designed the experiments. E. M. performed the experiments and analyzed the data. F. L. performed the synthesis of complex **5** and catalytic epoxidation reactions. M. L. performed X-ray analysis. E. M. and R. K. G. wrote the manuscript. All authors provided comments on the experiments and manuscript during its preparation.

Conflicts of interest

There are no conflicts to declare.

Acknowledgements

The European Commission is acknowledged for financial support through the NoNoMeCat project (675020-MSCA-ITN-2015-ETN). The China Scholarship Council is also acknowledged for financial support. We also thank Utrecht University. The X-ray diffractometer was financed by the Netherlands Organization for Scientific Research (NWO).

References

- 1 M. C. White and J. Zhao, *J. Am. Chem. Soc.*, 2018, **140**, 13988–14009.
- 2 B. Hong, T. Luo and X. Lei, *ACS Cent. Sci.*, 2020, **6**, 622–635.
- 3 K. Feng, R. E. Quevedo, J. T. Kohrt, M. S. Oderinde, U. Reilly and M. C. White, *Nature*, 2020, **580**, 621–627.
- 4 L. Que and W. B. Tolman, *Nature*, 2008, **455**, 333–340.
- 5 J. T. Groves and P. Viski, *J. Am. Chem. Soc.*, 1989, **111**, 8537–8538.
- 6 K. Srinivasan, P. Michaud and J. K. Kochi, *J. Am. Chem. Soc.*, 1986, **108**, 2309–2320.
- 7 J. T. Groves and P. Viski, *J. Org. Chem.*, 1990, **55**, 3628–3634.
- 8 K. Hamachi, R. Irie and T. Katsuki, *Tetrahedron Lett.*, 1996, **37**, 4979–4982.
- 9 T. Hamada, R. Irie, J. Mihara, K. Hamachi and T. Katsuki, *Tetrahedron*, 1998, **54**, 10017–10028.
- 10 A. Miyafuji and T. Katsuki, *Tetrahedron*, 1998, **54**, 10339–10348.
- 11 N. Komiya, S. Noji and S.-I. Murahashi, *Tetrahedron Lett.*, 1998, **39**, 7921–7924.
- 12 R. Zhang, W.-Y. Yu, T.-S. Lai and C.-M. Che, *Chem. Commun.*, 1999, 1791–1792.
- 13 S. I. Murahashi, S. Noji and N. Komiya, *Adv. Synth. Catal.*, 2004, **346**, 195–198.
- 14 R. Zhang, W.-Y. Yu and C.-M. Che, *Tetrahedron: Asymmetry*, 2005, **16**, 3520–3526.
- 15 S.-I. Murahashi, S. Noji, T. Hirabayashi and N. Komiya, *Tetrahedron: Asymmetry*, 2005, **16**, 3527–3535.
- 16 P. Le Maux, H. F. Srouf and G. Simonneaux, *Tetrahedron*, 2012, **68**, 5824–5828.



- 17 F. Burg, M. Gicquel, S. Breitenlechner, A. Pöthig and T. Bach, *Angew. Chem., Int. Ed.*, 2018, **57**, 2953–2957.
- 18 F. Burg, S. Breitenlechner, C. Jandl and T. Bach, *Chem. Sci.*, 2020, **11**, 2121–2129.
- 19 T. Nagataki, Y. Tachi and S. Itoh, *J. Mol. Catal. A: Chem.*, 2005, **225**, 103–109.
- 20 Y. Mekmouche, C. Duboc-Toia, S. Ménage, C. Lambeaux and M. Fontecave, *J. Mol. Catal. A: Chem.*, 2000, **156**, 85–89.
- 21 M. Milan, M. Bietti and M. Costas, *ACS Cent. Sci.*, 2017, **3**, 196–204.
- 22 G. Olivo, O. Cussó and M. Costas, *Chem. – Asian J.*, 2016, **11**, 3148–3158.
- 23 G. Olivo, O. Cussó, M. Borrell and M. Costas, *J. Biol. Inorg. Chem.*, 2017, **22**, 425–452.
- 24 E. P. Talsi, D. G. Samsonenko and K. P. Bryliakov, *ChemCatChem*, 2017, **9**, 2599–2607.
- 25 M. Milan, M. Bietti and M. Costas, *Org. Lett.*, 2018, **20**, 2720–2723.
- 26 R. V. Ottenbacher, E. P. Talsi, T. V. Rybalova and K. P. Bryliakov, *ChemCatChem*, 2018, **10**, 5323–5330.
- 27 B. Qiu, D. Xu, Q. Sun, C. Miao, Y.-M. Lee, X.-X. Li, W. Nam and W. Sun, *ACS Catal.*, 2018, **8**, 2479–2487.
- 28 B. Qiu, D. Xu, Q. Sun, J. Lin and W. Sun, *Org. Lett.*, 2019, **21**, 618–622.
- 29 X.-X. Li, M. Guo, B. Qiu, K.-B. Cho, W. Sun and W. Nam, *Inorg. Chem.*, 2019, **58**, 14842–14852.
- 30 M. Cianfanelli, G. Olivo, M. Milan, R. J. M. Klein Gebbink, X. Ribas, M. Bietti and M. Costas, *J. Am. Chem. Soc.*, 2019, **142**, 1584–1593.
- 31 Q. Sun and W. Sun, *Org. Lett.*, 2020, **22**, 9529–9533.
- 32 R. V. Ottenbacher, E. P. Talsi and K. P. Bryliakov, *J. Catal.*, 2020, **390**, 170–177.
- 33 R. V. Ottenbacher, A. A. Bryliakova, M. V. Shashkov, E. P. Talsi and K. P. Bryliakov, *ACS Catal.*, 2021, **11**, 5517–5524.
- 34 L. Vicens, M. Bietti and M. Costas, *Angew. Chem., Int. Ed.*, 2021, **60**, 4740–4746.
- 35 K. P. Bryliakov, *Chem. Rev.*, 2017, **117**, 11406–11459.
- 36 M. Milan, M. Bietti and M. Costas, *Chem. Commun.*, 2018, **54**, 9559–9570.
- 37 L. Vicens, G. Olivo and M. Costas, *ACS Catal.*, 2020, **10**, 8611–8631.
- 38 R. V. Ottenbacher, E. P. Talsi and K. P. Bryliakov, *Chem. Rec.*, 2018, **18**, 78–90.
- 39 M. Wu, B. Wang, S. Wang, C. Xia and W. Sun, *Org. Lett.*, 2009, **11**, 3622–3625.
- 40 R. V. Ottenbacher, K. P. Bryliakov and E. P. Talsi, *Adv. Synth. Catal.*, 2011, **353**, 885–889.
- 41 I. Garcia-Bosch, L. Gomez, A. Polo, X. Ribas and M. Costas, *Adv. Synth. Catal.*, 2012, **354**, 65–70.
- 42 O. Y. Lyakin, R. V. Ottenbacher, K. P. Bryliakov and E. P. Talsi, *ACS Catal.*, 2012, **2**, 1196–1202.
- 43 O. Cussó, I. Garcia-Bosch, D. Font, X. Ribas, J. Lloret-Fillol and M. Costas, *Org. Lett.*, 2013, **15**, 6158–6161.
- 44 N. C. Maity, P. K. Bera, D. Ghosh, S. H. Abdi, R. I. Kureshy, H. K. Noor-ul, H. C. Bajaj and E. Suresh, *Catal. Sci. Technol.*, 2014, **4**, 208–217.
- 45 R. V. Ottenbacher, D. G. Samsonenko, E. P. Talsi and K. P. Bryliakov, *ACS Catal.*, 2014, **4**, 1599–1606.
- 46 D. Shen, C. Miao, S. Wang, C. Xia and W. Sun, *Eur. J. Inorg. Chem.*, 2014, **2014**, 5777–5782.
- 47 C. Miao, B. Wang, Y. Wang, C. Xia, Y.-M. Lee, W. Nam and W. Sun, *J. Am. Chem. Soc.*, 2016, **138**, 936–943.
- 48 R. V. Ottenbacher, D. G. Samsonenko, E. P. Talsi and K. P. Bryliakov, *ACS Catal.*, 2016, **6**, 979–988.
- 49 D. Shen, B. Qiu, D. Xu, C. Miao, C. Xia and W. Sun, *Org. Lett.*, 2016, **18**, 372–375.
- 50 X. Chen, B. Gao, Y. Su and H. Huang, *Adv. Synth. Catal.*, 2017, **359**, 2535–2541.
- 51 J. Du, C. Miao, C. Xia, Y.-M. Lee, W. Nam and W. Sun, *ACS Catal.*, 2018, **8**, 4528–4538.
- 52 W. Wang, Q. Sun, C. Xia and W. Sun, *Chin. J. Chem.*, 2018, **39**, 1463–1469.
- 53 C. Clarasó, L. Vicens, A. Polo and M. Costas, *Org. Lett.*, 2019, **21**, 2430–2435.
- 54 D. Xu, Q. Sun, J. Lin and W. Sun, *Chem. Commun.*, 2020, **56**, 13101–13104.
- 55 R. Ottenbacher, V. Kurganskiy, E. Talsi and K. P. Bryliakov, *Adv. Synth. Catal.*, 2021, **363**, 2778–2782.
- 56 M. Wu, C. X. Miao, S. Wang, X. Hu, C. Xia, F. E. Kuehn and W. Sun, *Adv. Synth. Catal.*, 2011, **353**, 3014–3022.
- 57 O. Cussó, I. Garcia-Bosch, X. Ribas, J. Lloret-Fillol and M. Costas, *J. Am. Chem. Soc.*, 2013, **135**, 14871–14878.
- 58 O. Cussó, X. Ribas, J. Lloret-Fillol and M. Costas, *Angew. Chem., Int. Ed.*, 2015, **54**, 2729–2733.
- 59 O. Cussó, M. Cianfanelli, X. Ribas, R. J. M. Klein Gebbink and M. Costas, *J. Am. Chem. Soc.*, 2016, **138**, 2732–2738.
- 60 A. M. Zima, O. Y. Lyakin, R. V. Ottenbacher, K. P. Bryliakov and E. P. Talsi, *ACS Catal.*, 2016, **6**, 5399–5404.
- 61 W. Wang, Q. Sun, D. Xu, C. Xia and W. Sun, *ChemCatChem*, 2017, **9**, 420–424.
- 62 O. Cussó, X. Ribas and M. Costas, *Chem. Commun.*, 2015, **51**, 14285–14298.
- 63 J. Chen, Z. Jiang, S. Fukuzumi, W. Nam and B. Wang, *Coord. Chem. Rev.*, 2020, **421**, 213443.
- 64 B. P. Roberts, *Chem. Soc. Rev.*, 1999, **28**, 25–35.
- 65 M. Salamone and M. Bietti, *Acc. Chem. Res.*, 2015, **48**, 2895–2903.
- 66 D. Wang, W. G. Shuler, C. J. Pierce and M. K. Hilinski, *Org. Lett.*, 2016, **18**, 3826–3829.
- 67 E. Gaster, S. Kozuch and D. Pappo, *Angew. Chem., Int. Ed.*, 2017, **56**, 5912–5915.
- 68 V. Dantignana, M. Milan, O. Cussó, A. Company, M. Bietti and M. Costas, *ACS Cent. Sci.*, 2017, **3**, 1350–1358.
- 69 J. P. Lumb, *Angew. Chem., Int. Ed.*, 2017, **56**, 9276–9277.
- 70 M. Borrell, S. Gil-Caballero, M. Bietti and M. Costas, *ACS Catal.*, 2020, **10**, 4702–4709.
- 71 E. Masferrer-Rius, R. M. Hopman, J. van der Kleij, M. Lutz and R. J. M. Klein Gebbink, *Chimia*, 2020, **74**, 489–494.
- 72 E. P. Talsi, D. G. Samsonenko, R. V. Ottenbacher and K. P. Bryliakov, *ChemCatChem*, 2017, **9**, 4580–4586.



- 73 E. Masferrer-Rius, M. Borrell, M. Lutz, M. Costas and R. J. M. Klein Gebbink, *Adv. Synth. Catal.*, 2021, **363**, 3783–3795.
- 74 A. M. Zima, O. Y. Lyakin, D. S. Bushmin, I. E. Soshnikov, K. P. Bryliakov and E. P. Talsi, *Mol. Catal.*, 2021, **502**, 111403.
- 75 A. M. Zima, O. Y. Lyakin, K. P. Bryliakov and E. P. Talsi, *Chem. – Eur. J.*, 2021, **27**, 7781–7788.
- 76 G. Olivo, O. Lanzalunga, L. Mandolini and S. Di Stefano, *J. Org. Chem.*, 2013, **78**, 11508–11512.
- 77 I. Kaljurand, A. Kütt, L. Sooväli, T. Rodima, V. Mäemets, I. Leito and I. A. Koppel, *J. Org. Chem.*, 2005, **70**, 1019–1028.
- 78 J. G. Małecki and A. Maroń, *Transition Met. Chem.*, 2013, **38**, 133–142.
- 79 CCDC 2100950 and 2100951 contain the supplementary crystallographic data for this paper.
- 80 U. Knof and A. von Zelewsky, *Angew. Chem., Int. Ed.*, 1999, **38**, 302–322.
- 81 Y. Zang, J. Kim, Y. Dong, E. C. Wilkinson, E. H. Appelman and L. Que, *J. Am. Chem. Soc.*, 1997, **119**, 4197–4205.
- 82 V. A. Yazerski, P. Spanring, D. Gatineau, C. H. Woerde, S. M. Wiclawska, M. Lutz, H. Kleijn and R. J. M. Klein Gebbink, *Org. Biomol. Chem.*, 2014, **12**, 2062–2070.
- 83 B. Wang, C. Miao, S. Wang, C. Xia and W. Sun, *Chem. – Eur. J.*, 2012, **18**, 6750–6753.
- 84 B. Wang, S. Wang, C. Xia and W. Sun, *Chem. – Eur. J.*, 2012, **18**, 7332–7335.
- 85 R. V. Ottenbacher, E. P. Talsi and K. P. Bryliakov, *ACS Catal.*, 2015, **5**, 39–44.
- 86 E. P. Talsi, R. V. Ottenbacher and K. P. Bryliakov, *J. Organomet. Chem.*, 2015, **793**, 102–107.
- 87 W. Sun and Q. Sun, *Acc. Chem. Res.*, 2019, **52**, 2370–2381.
- 88 O. Y. Lyakin, A. M. Zima, N. V. Tkachenko, K. P. Bryliakov and E. P. Talsi, *ACS Catal.*, 2018, **8**, 5255–5260.
- 89 N. V. Tkachenko, R. V. Ottenbacher, O. Y. Lyakin, A. M. Zima, D. G. Samsonenko, E. P. Talsi and K. P. Bryliakov, *ChemCatChem*, 2018, **10**, 4052–4057.
- 90 N. V. Tkachenko, O. Y. Lyakin, A. M. Zima, E. P. Talsi and K. P. Bryliakov, *J. Organomet. Chem.*, 2018, **871**, 130–134.
- 91 A. M. Zima, O. Y. Lyakin, D. P. Lubov, K. P. Bryliakov and E. P. Talsi, *Mol. Catal.*, 2020, **483**, 110708.
- 92 M. Mitra, O. Cussó, S. S. Bhat, M. Sun, M. Cianfanelli, M. Costas and E. Nordlander, *Dalton Trans.*, 2019, **48**, 6123–6131.
- 93 E. P. Talsi and K. P. Bryliakov, *Coord. Chem. Rev.*, 2012, **256**, 1418–1434.
- 94 K. P. Bryliakov and E. P. Talsi, *Coord. Chem. Rev.*, 2014, **276**, 73–96.
- 95 J. Chen and R. J. M. Klein Gebbink, *ACS Catal.*, 2019, **9**, 3564–3575.
- 96 M. R. Bukowski, S. Zhu, K. D. Koehntop, W. W. Brennessel and L. Que, *JBIC, J. Biol. Inorg. Chem.*, 2004, **9**, 39–48.
- 97 D. Pijper, P. Saisaha, J. W. de Boer, R. Hoen, C. Smit, A. Meetsma, R. Hage, R. P. van Summeren, P. L. Alsters and B. L. Feringa, *Dalton Trans.*, 2010, **39**, 10375–10381.
- 98 C. Miao, X.-X. Li, Y.-M. Lee, C. Xia, Y. Wang, W. Nam and W. Sun, *Chem. Sci.*, 2017, **8**, 7476–7482.
- 99 Y.-R. Luo, *Comprehensive handbook of chemical bond energies*, CRC press, 2007.

